

# Fatigue Delamination Growth Under Cyclic Compression in Glass/Epoxy Composite Beam/Plates

G. A. KARDOMATEAS\* and B. MALIK

*School of Aerospace Engineering  
Georgia Institute of Technology  
Atlanta, Georgia 30332-0150*

Results are reported on the fatigue growth of internal delaminations in glass/epoxy composite beam/plates subjected to constant amplitude cyclic compression. Because of compressive loading, these structures undergo repeated buckling/unloading of the delaminated layer with a resulting reduction of the interlayer resistance. A noteworthy feature of the problem is that the state of stress near the delamination tip is of mixed mode (I and II). The present combined experimental/analytical investigation for the glass/epoxy composites complements our earlier studies on delamination growth under cyclic compression in unidirectional graphite/epoxy specimens. Several configurations are studied with the delamination located at different depths (through the thickness) and with different applied maximum compressive displacements. The experimental data are correlated with the predictions from a combined delamination buckling/postbuckling and fracture mechanics model. A mode-dependent fatigue delamination growth law is used together with an initial postbuckling solution for the deformation pattern of the delaminated layer and the substrate, which does not impose any restrictive assumptions on the delamination thickness and plate length. The experimental data seem to be adequately correlated with the theory and the fatigue delamination growth is found again to be strongly affected by the relative location of the delamination through the plate thickness. Finally, a comparison of the cyclic growth rate in glass/epoxy specimens with the corresponding one in graphite/epoxy specimens of the same geometry and applied loading shows that the delamination would grow much faster in the graphite/epoxy specimens.

## INTRODUCTION

The confident use of layered composites in engineering structures requires knowledge of the response and failure characteristics under different loading conditions. Equally important is the knowledge of the behavior of the structure in the presence of defects. One of the more common failures is the formation of internal delaminated zones, i.e., two adjacent layers are partially debonded at their interface. This is generally a consequence of low-velocity impact or because of pre-existing manufacturing imperfections.

Under compression loading, the delaminated layer may buckle. This local instability does not necessarily imply failure, and usually the laminate is capable of carrying on in the postbuckling phase under higher loading. However, the buckling-induced stresses at the tip of the delamination may cause growth of the

interlayer crack and eventual complete separation of the layer. Besides strength and stiffness, delaminations can influence other performance characteristics, such as the energy absorption capacity of composite beam systems (1).

The growth characteristics of the delamination can be investigated once a postbuckling solution is available. Therefore, a combined fracture mechanics analysis and delamination postbuckling solution is needed. This is a nontraditional problem in fracture mechanics since the determination of the postbuckling deflections of a thin debonded layer when a plate element is subjected to axial compression is geometrically nonlinear and includes the explicit presence of additional parameters with the dimension of the length (e.g., the thickness of the separated layer or the plate length).

Accordingly, this subject of delamination buckling and growth has become the topic of numerous publications (2-6). Experiments on the monotonic growth of delaminations under delamination buckling condi-

\* To whom correspondence should be addressed.

tions were conducted by Kardomateas (7) whereas Russell and Street (8, 9) performed experiments on graphite/epoxy specimens under pure Mode I or pure Mode II loading.

One characteristic of delaminations in composites is that, being essentially interlaminar cracks, they are constrained to move on a specific plane (along the layer interface), unlike macro-cracks in metals which can change direction. Therefore, delaminations grow under a state of mixed mode, I and II, often with a high Mode II content, unlike macro-cracks in metals which normally change direction and eventually turn into Mode I cracks. Accordingly, an important issue is the extent to which the fracture toughness is dependent on the mode mixity (ratio of mode II to mode I). Recent experimental studies on several composites have clearly shown that a mode-independent approach would be inadequate (10, 11).

As has been mentioned, an initial postbuckling solution for the delaminated composite is necessary for proper correlation with the test data. To this extent, Kardomateas (12) provided a closed form solution for the initial postbuckling behavior of delaminated composites without imposing any restrictive assumptions on the delamination or specimen dimensions. The solution was derived through a perturbation procedure based on an asymptotic expansion of the load and deformation quantities in terms of the distortion parameter of the delaminated layer, the latter being considered a compressive elastica. An extended analysis considered the effects of the end conditions, i.e. clamped-clamped or simply-supported (13). Subsequently, the bimaterial interface crack solutions for the mode mixity and the energy release rate in terms of the resultant moments and forces, as derived by Suo and Hutchinson (14) were employed. These relations are actually simplified because the material is assumed homogeneous. These formulas are adequate because we are dealing with a macroscopically homogeneous material (unidirectional glass/epoxy). Notice that an expression for the total energy release rate in terms of the resultant forces and moments at the delamination tip had been given earlier by Yin and Wang (15). Also, recently, Sheinman and Kardomateas (16) have developed an extended new set of formulas for the total energy release rate and the decomposition into its Mode I and Mode II components, which are valid for general non-homogeneous laminated composites with arbitrary stacking sequence.

The postbuckling solution by Kardomateas (12) was used in a subsequent study (17) for the stability of growth of internal delaminations, i.e. to define the combinations of delamination length and applied strain that lead to unstable growth; this would practically cause either contained "jump" growth or catastrophic (complete) growth of the delamination. A major conclusion of that study was that delamination growth is more likely to be stable than would be predicted by the thin film model. The present study complements the recent one by Kardomateas *et al.* (18), in which an experimental investigation was conducted

on the growth of internal delaminations in graphite/epoxy composite plates subjected to cyclic compression. In the latter study a mixed-mode cyclic growth law was proposed and was found to correlate adequately with the test data. The growth law is a function of the spread in the energy release rate in the pre- and postbuckled states and the maximum value of the energy release rate in the cycle, both normalized with the mode-dependent interface fracture toughness. The exponent and the constant of the growth law are also taken to be mode-dependent.

In the present paper, the fatigue growth of delaminations in glass/epoxy composites under constant amplitude cyclic compression is studied by conducting experiments on several specimen configurations with the initial delaminations of different lengths located at different sites through the thickness, and at different applied maximum compressive strains. The test data are correlated with the theory, which does not impose any restrictive assumptions regarding the delamination thickness and plate length (as opposed to the usual thin film assumptions). Also, a comparison is made between the cyclic growth rate in glass/epoxy and graphite/epoxy.

## EXPERIMENTAL PROCEDURES

### Material and Specimens

The glass/epoxy used in this study was the S2/SP250 made by 3M Co., and was supplied in the form of prepreg tape by NASA Langley. The average ply thickness of the S2/SP250 was 0.2413 mm and the mechanical properties of this material are as follows: moduli (in GPa)  $E_L = 45.5$ ,  $E_T = 14.5$ ,  $G_{LT} = 4.13$ ; in-plane Poisson's ratio  $\nu_{LT} = 0.26$ ; resin content  $33 \pm 3$  wt%. The specimens were made by hand lay-up and curing in the autoclave according to the cure cycle provided by the manufacturer of the prepreg tape, namely at a temperature of 120°C (250°F) and a pressure of 50 psi (a vacuum bag was placed prior to applying the curing cycle). The cured laminates which were 304.8 by 50.8 mm (12 by 2 inches), were carefully inspected for possible abnormalities and were subsequently cut into 152.4 by 12.7 mm (6 by 0.5 inch) pieces using a tungsten-carbide tipped tool.

The delaminations were introduced by placing at the desired location through the width a DuPont Teflon film of 0.0254 mm (0.001 inch) thickness. The thickness of the insert which would simulate a real time delamination is very important. A thick implanted insert can produce a resin rich pocket in front of the implanted delamination which would result in high resistance to the initial growth of the delamination. The existence of this resin rich pocket can distort the experimental data. Some documentation already exists on the subject of resin rich pockets and their effects on fracture toughness testing. A study by Murri and Martin (19) showed that the required applied loading for propagation of a crack from an insert decreases with decreasing insert thickness. In that study, the magnified photographic views of the pre-

crack surfaces with different thicknesses of insert clearly demonstrate the relationship between insert thickness and size of the resin rich pocket. In the same study it was concluded that use of an insert thickness of 13  $\mu\text{m}$  (0.0005 inch) for pre-cracking does not produce a resin pocket as compared to the insert of 75  $\mu\text{m}$  (0.0019 inch).

Since the curing process affects the final dimensions of the specimens as the result of resin bleeding, the thicknesses of the specimens were measured after curing with a micrometer. At this point it should be mentioned that the preparation of the glass/epoxy specimens required more effort and care than the graphite/epoxy ones because of the larger ply thicknesses and the different resin flow properties. It is also recommended to make laminates of greater length than required, so that a finished specimen that does not have appreciable variation in thickness at each cross section can be easily identified and cut. In our specimens, the thickness measurements were taken at different points through the width and length to insure overall uniformity of the thickness and they were found to be satisfactory. Specimens were tested in compression at moderate load and displacement levels. Compressive testing is often done by using tabs or an interleaf between the specimen and the jaws of the testing machine in order to better transmit the applied load to the specimen through friction. Neither tabs nor interleafs were found to be needed. The tabless specimens used in this experimental study proved to be very effective, besides being less expensive and requiring less time.

Testing in compression fatigue was carried out in an Instron 8500 servo-hydraulic testing system. The experiments were done in displacement control. A sine wave of 5 Hz was applied. Delamination growth was monitored using a Questar remote video-measurement system, which includes a traveling microscope.

The toughness properties and fatigue growth parameters were: critical energy release rates,  $G_{ic} = 134 \text{ N/m}$ ,  $\lambda = G_{ic}/G_{IIC} = 0.223$ ; and exponent ratio,  $\mu = m_{II}/m_I = 1.75$ , constant ratio,  $\kappa = C_{II}/C_I = 10.50$ . These constants for the glass/epoxy material were found from independent Mode I and Mode II tests and have been reported (19-21). Alternatively, the present mixed mode buckling-induced fatigue delamination growth data could be used to determine these constants. The definition of these constants is also discussed in the next section. The specimens had a width,  $w = 12.7 \text{ mm}$ , and a slightly varying half-length between the grips,  $L$ , between 50 and 60 mm, as indicated in the Tables of the results.

#### Fatigue Delamination Growth Data and Analysis

The specimens consisted of 24 plies with the delamination implanted either between the fourth and fifth ply (4/24) or between the fifth and sixth ply (5/24). Different applied maximum compressive strains and different initial delamination lengths were used, which resulted in the following test configurations:

- (a) 5/24 A: 24 plies, specimen thickness  $T = 4.98 \text{ mm}$ , specimen half-length between grips  $L = 57.6 \text{ mm}$ , initial delamination of half-length  $\ell_0 = 26.607 \text{ mm}$ , between fifth and sixth ply, hence  $h/T = 5/24$ , and at a maximum compressive strain  $\epsilon_{max} = 2.281 \times 10^{-3}$ . The delamination extended in fatigue up to half-length of  $\ell = 37.173 \text{ mm}$  requiring 281,371 cycles.
- (b) 5/24 B: 24 plies, specimen thickness  $T = 4.98 \text{ mm}$ , specimen half-length between grips  $L = 54.6 \text{ mm}$ , initial delamination of half-length  $\ell_0 = 31.255 \text{ mm}$ , between fifth and sixth ply ( $h/T = 5/24$ ), and at a maximum compressive strain  $\epsilon_{max} = 3.004 \times 10^{-3}$ . Delamination extension up to  $\ell = 37.871 \text{ mm}$  in 54,675 cycles.
- (c) 5/24 C: 24 plies, specimen thickness  $T = 4.98 \text{ mm}$ , specimen half-length between grips  $L = 58.4 \text{ mm}$ , initial delamination of half-length  $\ell_0 = 23.927 \text{ mm}$ , between fifth and sixth ply, hence  $h/T = 5/24$ , and at a maximum compressive strain  $\epsilon_{max} = 2.681 \times 10^{-3}$ . Delamination extension up to  $\ell = 31.255 \text{ mm}$  in 71,504 cycles.
- (d) 4/24 A: 24 plies, specimen thickness  $T = 4.98 \text{ mm}$ , specimen half-length between grips  $L = 55.6 \text{ mm}$ , initial delamination of half-length  $\ell_0 = 25.514 \text{ mm}$ , between fourth and fifth ply ( $h/T = 4/24$ ), and at a maximum compressive strain  $\epsilon_{max} = 2.354 \times 10^{-3}$ . In this configuration the delamination extended in fatigue up to  $\ell = 27.775 \text{ mm}$  in 252,260 cycles.
- (e) 4/24 B: 24 plies, specimen thickness  $T = 5.10 \text{ mm}$ , specimen half-length between grips  $L = 56.0 \text{ mm}$ , initial delamination of half-length  $\ell_0 = 22.428 \text{ mm}$ , between fourth and fifth ply ( $h/T = 4/24$ ), and at a maximum compressive strain  $\epsilon_{max} = 2.338 \times 10^{-3}$ . In this configuration the delamination extended in fatigue up to  $\ell = 30.099 \text{ mm}$  in 406,724 cycles.

These five test configurations exhibit different mode mixities and energy release rates at  $\epsilon_{max}$ . It should be mentioned that the applied maximum strain,  $\epsilon_{max}$ , is in all cases below the level that would cause growth of the delaminations in a monotonic test.

The mode dependence of the fracture toughness is now a well accepted notion and it has been demonstrated experimentally by Chai (11) and the experiments of Russell and Street (8, 9). In a related study on glass/epoxy, Liechti and Chai (22) measured the toughness of the glass/epoxy interface over a wide range of mode mixes and found a toughening effect associated with increasing in-plane shear components. Furthermore, optical interference measurements of the normal crack opening displacement that were made near the crack front revealed large variations in plastic zone size with mode mix. The plastic zone sizes followed the same trends that the toughness exhibited with mode mix. Although all yielding was small scale in nature, there were large increases in size as the shear component increased.

To account for the existence of both Modes I and II, the mode mixity,  $\psi$  is defined by

$$\psi = \tan^{-1} (K_{II} / K_I) \quad (1)$$

A pure Mode II state would result in  $\psi = \pm 90^\circ$  and a pure Mode I state in  $\psi = 0^\circ$ .

A simple, one parameter family of mixed mode adjusted fracture criteria has been described by Hutchinson and Suo (23):

$$\Gamma_0(\psi) = G_{Ic} [1 + (\lambda - 1) \sin^2 \psi]^{-1}; \lambda = G_{Ic} / G_{IIc} \quad (2)$$

where  $G_{Ic}$ ,  $G_{IIc}$  are the values of the pure Mode I and pure Mode II toughness, respectively. The parameter  $\lambda$  accounts for the influence of the mode II contribution in the criterion. For Mode I,  $\psi = 0$ ,  $\Gamma_0 = G_{Ic}$  and at Mode II,  $\psi = \pm 90^\circ$ ,  $\Gamma_0 = G_{IIc}$ . Notice that the limit  $\lambda = 1$  is the case of the classical mode-independent toughness, i.e.,  $\Gamma_0 = G_{Ic}$  for all mode combinations.

Returning to the delamination growth in the initial postbuckling phase during cyclic compression, the effects of mode-dependent toughness on the growth characteristics can be accounted for by normalizing the energy release rate with the mode-dependent toughness, i.e., by defining (18):

$$\bar{G} = \frac{G}{\Gamma_0(\psi)} = \bar{G}(\epsilon_0, \psi) \quad (3)$$

Then  $\bar{G}$  can be regarded as a mode-adjusted crack driving force in the sense that the criterion for crack advance is  $\bar{G} = G / \Gamma_0(\psi) = 1$ .

The mode mixity and the energy release rate at a given applied strain can be determined by using the initial postbuckling solution, which is outlined in the next section. Figure 1a shows the mode mixity,  $\psi$ , at  $\epsilon_{max}$ , as a function of the delamination length,  $\ell$ , for the five glass/epoxy specimen configurations considered. A value of  $\psi = -90^\circ$  means pure Mode II. Initially, the mode mixity at the delamination tip is between  $-55^\circ$  and  $-65^\circ$ , and it decreases in all cases as the delamination grows, which means that an increasingly higher Mode II component exists.

Figure 1b shows the energy release rate,  $G$ , at  $\epsilon_{max}$ , normalized with the mode-dependent fracture toughness,  $\Gamma_0(\psi)$ , as a function of the delamination length,  $\ell$ . Initially, the 5/24 specimens are subjected to an energy release rate between 68% and 48% of the critical value, and the 4/24 specimens are subjected to an energy release rate <38% of the critical value. The energy release rate is decreasing in all cases as the delamination grows under constant compressive amplitude  $\epsilon_{max}$ .

Prediction of the cyclic growth, i.e. delamination extension versus number of compression cycles requires use of a cyclic growth law. The following general power law relation was postulated in Kardomateas *et al.* (18) for the cyclic delamination growth:

$$\frac{da}{dN} = C(\psi) \frac{(\Delta \bar{G})^{m(\psi)}}{1 - \bar{G}_{max}} \quad (4)$$

$\Delta \bar{G}$  is the range in the energy release rate (normalized with the mode-dependent fracture toughness),  $\Delta \bar{G} = \bar{G}_{max} - \bar{G}_{min}$ . The denominator was introduced to model the very short life (typically  $<10^3$  cycles), near the fracture toughness region. However, outside this region the denominator has a negligible influence. The well-known Paris fatigue law in metals has a similar power law structure but uses the stress intensity factor  $\Delta K$  for a single pure mode.

This fatigue growth law should be valid above a threshold level, i.e., there is a threshold value  $\Delta \bar{G}_{thr}$  below which delamination growth in fatigue does not take place. Bathias and Laksimi (24) have investigated experimentally the fatigue threshold for glass/epoxy and they found a  $\Delta \bar{G}_{thr}$  in Mode I about one sixth of the critical value  $G_{Ic}$ . This indicates the importance of the threshold in polymeric matrix composites by comparison with metals because in numerous alloys the difference can be as high as a factor of 100.

The mode-dependence of the  $C$  and  $m$  constants in the growth law has been demonstrated experimentally by Russell and Street (8, 9). Of the two parameters, the most important is the exponent,  $m$ . Following the format of Eq 2 for the mode-dependence of the fracture toughness, Kardomateas *et al.* (18) set:

$$m(\psi) = m_I [1 + (\mu - 1) \sin^2 \psi]; \mu = m_{II} / m_I \quad (5)$$

where, again at pure Mode I,  $\psi = 0$ ,  $m = m_I$  and at pure Mode II,  $\psi = \pm 90^\circ$ ,  $m = m_{II}$ .

In a similar fashion, the parameter  $C(\psi)$  in (4) was set, following the same structure as Eq 2 for the mode-dependent fracture toughness,

$$C(\psi) = C_I [1 + (\kappa - 1) \sin^2 \psi]; \kappa = C_{II} / C_I \quad (6)$$

where  $C_I$  is the constant  $C$  at pure Mode I and  $\kappa$  is defined as the ratio of the constant  $C$  at Modes II and I.

These constants can be determined independently. Specifically, Mode II fatigue testing can be carried out by using end-delaminated flexure specimens as in Russell and Street (8). Pure Mode I fatigue testing can be carried out by using a uniform width and thickness double-cantilever-beam specimen (9). These tests would allow determining  $C_{I,II}$ ,  $m_{I,II}$  and hence  $\mu$  and  $\kappa$ . The same tests can be performed statically to allow measuring  $G_{Ic}$  and  $G_{IIc}$ , hence  $\lambda$ .

Regarding our tests on glass/epoxy specimens, two data points ( $\ell; N$ ) from the 5/24 A specimen were used to obtain the constants  $m_I$  and  $C_I$ . These data points are (29.604 mm; 51,601 cycles) and (37.173 mm; 281,371 cycles). The values obtained are:  $m_I = 1.0037$  and  $C_I = 0.1349 \times 10^{-7}$  m/cycle.

Based on these values, Figs. 2a and 2b show the actual experimental data and the predicted cycles for all five specimen configurations on a semi-logarithmic plot. The delamination in each experiment grew straight along the interface and its length was measured with the help of a remote optical telescope/video measurement system. It should be first emphasized that the same exponent and constant values in the

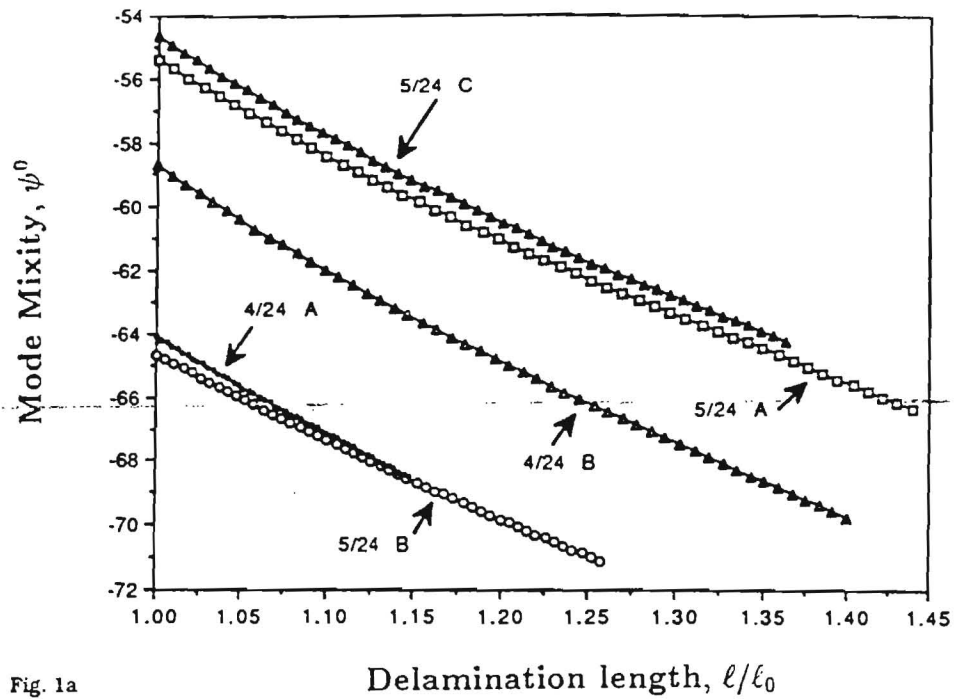


Fig. 1a. Mode mixity,  $\psi^\circ$ , versus delamination half-length,  $\ell/\ell_0$ , for the glass/epoxy specimen configurations tested ( $\ell_0$  is the initial delamination half-length). The pure Mode II is for  $\psi = \pm 90^\circ$ .  
 Fig. 1b. Maximum energy release rate,  $\bar{G}_{max} = G_{max}/\Gamma_0(\psi)$ , versus delamination half-length,  $\ell/\ell_0$ , for the glass/epoxy specimen configurations tested.

Fig. 1a

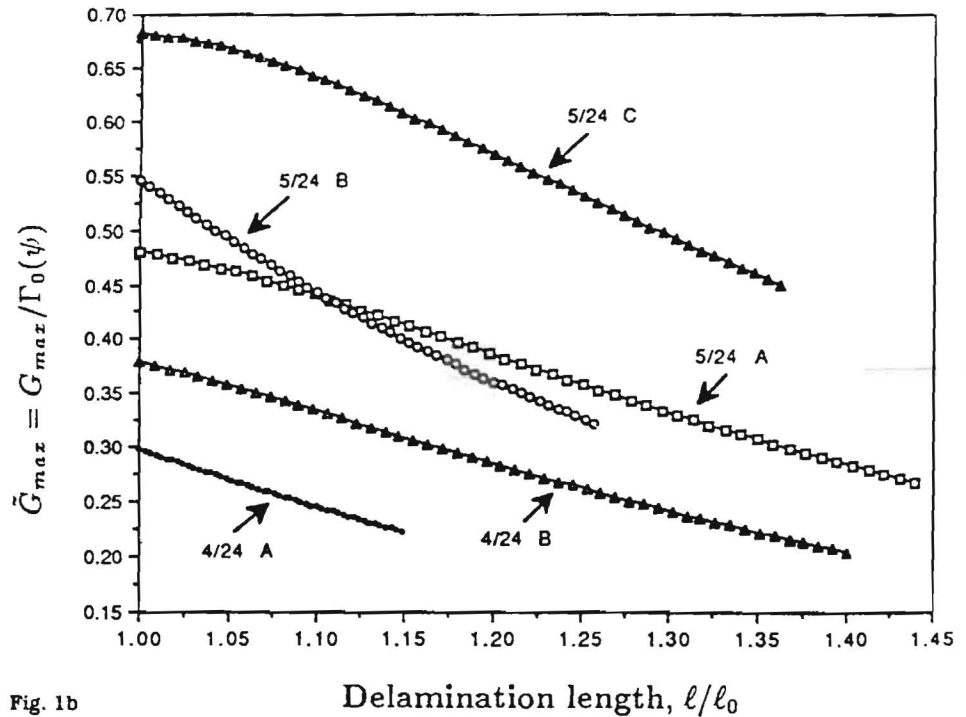


Fig. 1b

growth law are used for all delaminations, although each delamination configuration is characterized by a different location through the thickness, different initial length, different applied peak strain, and different mode mixity. Since measurements were performed at discrete points, the measured data are given by discrete data points, whereas the predictions are represented by the lines.

First, an immediate observation can be made by comparing the 5/24 C and the 4/24 B tests, which

have comparable ranges of delamination lengths and applied displacements, that the smaller the ratio  $h/T$  (delamination located closer to the surface), the slower the growth. Second, the experimental data seem to correlate adequately with the predicted values. For a more detailed record of the test data, Table 1 gives the actual experimental data and the predicted cycles for all five specimen configurations. Figure 2c shows a picture of an actual 5/24 A specimen undergoing cyclic compression (which causes delamination buck-

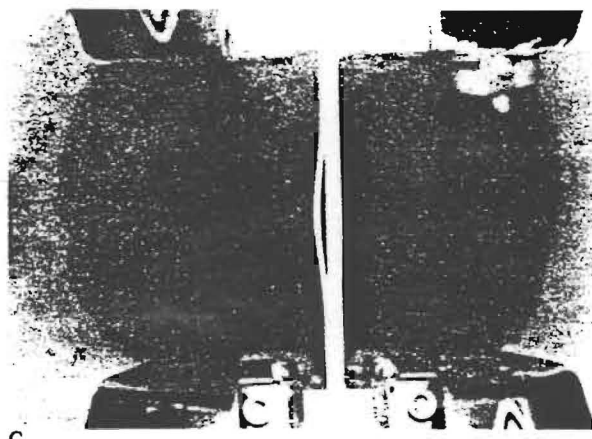
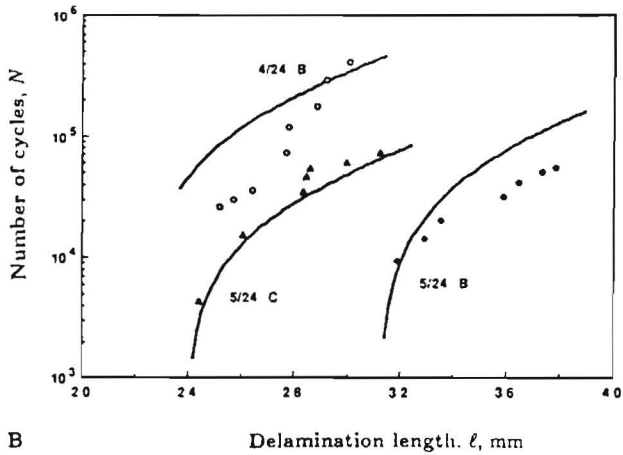
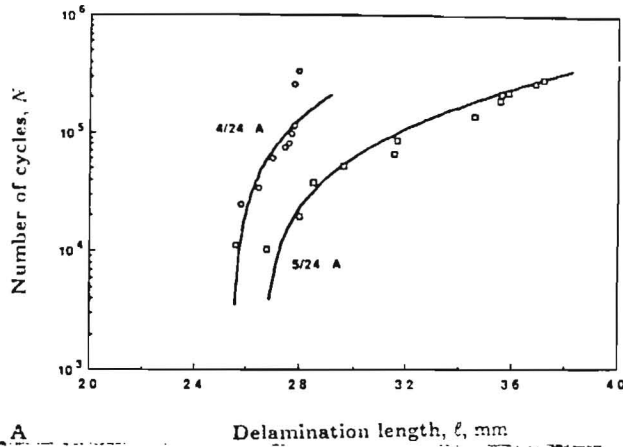


Fig. 2a. Fatigue delamination growth,  $N - \ell$  (semilogarithmic plot), for the 4/24 A and 5/24 A specimen configurations. In each case the experimental data are denoted with discrete marks, whereas the lines represent the predictions of the theory.  
 Fig. 2b. Fatigue delamination growth,  $N - \ell$  (semilogarithmic plot), for the 4/24 B, 5/24 B and 5/24 C specimen configurations (experimental data are denoted with discrete marks and the lines are the theoretical predictions).  
 Fig. 2c. An actual 4/24 A glass/epoxy specimen undergoing cyclic compression (which causes cyclic delamination buckling) at the point of peak compressive strain: the delamination has already grown by about 35 percent.

Table 1a. Comparison With Experiments: Glass/Epoxy,  $G_{Ic} = 134$ , N/m,  $\lambda = G_{Ic}/G_{IIc} = 0.223$  Growth Law:  $m_I = 1.004$  and  $C_I = 0.1349 \times 10^{-7}$  m/cycle  $\mu = m_{II}/m_I = 1.75$ ,  $\kappa = C_{II}/C_I = 10.5$ , See Eqs 1-6.

h/T Specimen Type	$\ell$ , mm Delamination Half-Length	$N_{theo}$ Cycles Predicted	$N_{exp}$ Cycles From Tests
5/24 A	26.746	2197	10,257
$\ell_0 = 26.607$ mm	28.004	22,715	19,572
$T = 4.98$ mm	28.512	31,472	37,167
$L = 57.4$ mm	29.604*	51,601	51,601*
$\epsilon_{max} = 2.281 \times 10^{-3}$	31.585	94,129	64,484
	31.661	95,950	84,662
	34.557	178,580	134,728
	35.560	214,416	185,630
	35.598	215,860	210,729
	35.865	226,185	217,431
	36.855	267,471	260,200
	37.173*	287,100	287,100*

\* Used to obtain  $m_I$  and  $C_I$ .

Table 1b. Comparison With Experiments: Glass/Epoxy,  $G_{Ic} = 134$ , N/m,  $\lambda = G_{Ic}/G_{IIc} = 0.223$  Growth Law:  $m_I = 1.004$  and  $C_I = 0.1349 \times 10^{-7}$  m/cycle  $\mu = m_{II}/m_I = 1.75$ ,  $\kappa = C_{II}/C_I = 10.5$ , See Eqs 1-6.

h/T Specimen Type	$\ell$ , mm Delamination Half-Length	$N_{theo}$ Cycles Predicted	$N_{exp}$ Cycles From Tests
5/24 B	31.902	7,012	9,361
$\ell_0 = 31.255$ mm	32.957	20,289	14,157
$T = 4.98$ mm	33.541	28,721	19,775
$L = 54.6$ mm	35.928	72,658	30,985
$\epsilon_{max} = 3.004 \times 10^{-3}$	36.462	84,873	40,451
	37.338	107,084	50,561
	37.871	122,015	54,675
5/24 C	24.397	2,696	4,376
$\ell_0 = 23.927$ mm	26.060	12,835	15,473
$T = 4.98$ mm	28.346	30,361	34,585
$L = 58.4$ mm	28.461	31,400	46,004
$\epsilon_{max} = 2.681 \times 10^{-3}$	28.588	32,570	53,598
	29.997	47,171	60,024
	31.255	63,126	71,504

ling) at the point of peak compressive strain; the delamination has already grown by ~35%).

The fatigue growth of delaminations under cyclic compression in graphite/epoxy specimens was studied in a recent article (18). In order to compare the growth rates for these two widely used classes of composites we refer to Figs. 3a and 3b. Figure 3a shows the predicted delamination length vs. number of cycles for two of the configurations that were studied experimentally in the latter article; and Fig. 3b shows the energy release rate versus delamination length at  $\epsilon_{max}$ . These configurations have the following details:

- (a) 4/30: 30 plies, specimen thickness  $T = 2.87$  mm, specimen half-length between grips  $L = 50.8$  mm, specimen width  $w = 12.7$  mm, delamination of half-length  $\ell_0 = 21.25$  mm, between fourth and fifth ply, hence  $h/T = 4/30$ , and at a maximum compressive strain  $\epsilon_{max} = 1.575 \times 10^{-3}$ .
- (b) 6/30: 30 plies, specimen thickness  $T = 2.75$  mm, delamination of half-length  $\ell_0 = 26.15$  mm, be-

Table 1c. Comparison With Experiments: Glass/Epoxy,  $G_{ic} = 134$ , N/m,  $\lambda = G_{ic}/G_{ic} = 0.223$  Growth Law:  $m_i = 1.004$  and  $C_i = 0.1349 \times 10^{-7}$  m/cycle  $\mu = m_{II}/m_I = 1.75$ ,  $\kappa = C_{II}/C_I = 10.5$ , See Eqs 1-6.

h/T Specimen Type	$\ell$ , mm Delamination Half-Length	$N_{theo}$ Cycles Predicted	$N_{exp}$ Cycles From Tests
<b>4/24 A</b>	25.552	1607	11,123
$\ell_0 = 25.514$ mm	25.781	11,484	24,873
$T = 4.98$ mm	26.454	42,521	33,443
$L = 55.6$ mm	26.937	66,794	59,540
$\epsilon_{max} = 2.354 \times 10^{-3}$	27.432	93,565	73,874
	27.584	102,193	80,906
	27.686	108,095	97,281
	27.750	111,844	113,958
	27.775	113,319	252,260
<b>4/24 B</b>	25.146	82,686	25,978
$\ell_0 = 22.428$ mm	25.654	101,545	29,799
$T = 5.10$ mm	26.416	132,466	35,417
$L = 56.0$ mm	27.686	192,141	71,565
$\epsilon_{max} = 2.338 \times 10^{-3}$	27.750	195,450	119,397
	28.829	256,172	178,400
	29.210	280,011	291,609
	30.099	341,084	406,724

tween sixth and seventh ply ( $h/T = 6/30$ ) and at a maximum compressive strain  $\epsilon_{max} = 1.325 \times 10^{-3}$ .

The material data for graphite/epoxy are the ones used by Kardomateas *et al.* (18): modulus of elasticity  $E_L = 151.6$  GPa; critical energy release rates,  $G_{ic} = 190$  N/m,  $\lambda = G_{ic}/G_{ic} = 0.30$ ; exponent ratio,  $\mu = m_{II}/m_I = 0.501$ , constant ratio,  $\kappa = C_{II}/C_I = 10.01$ , Mode I growth law exponent  $m_I = 10.385$  and Mode I growth law constant  $C_I = 0.0435$  m/cycle.

The results of Fig. 3a show clearly that the delamination in the graphite/epoxy would grow much faster than in the glass/epoxy material (the number of cycles differ by many orders of magnitude). Moreover, for the same applied  $\epsilon_{max}$ , the graphite/epoxy would be in a state of higher energy release rate values  $G/\Gamma_0(\psi)$  (Fig. 3b). The mode mixities, however, are nearly the same in both the glass/epoxy and graphite/epoxy cases. This demonstrates that in terms of fatigue delamination growth the glass/epoxy would be more growth resistant despite the lower initiation (toughness) values  $\Gamma_0(\psi)$ .

**Initial Postbuckling Analysis**

A closed form solution for the initial postbuckling solution in the general case (arbitrary delamination thickness or plate length) has been derived by Kardomateas (12). Referring to Fig. 4, consider a plate of half-length  $L$  (and unit width) with a through-the-width delamination of half-length  $\ell$ , symmetrically located. The delamination is at an arbitrary position through the thickness  $T$ . Over the delaminated region, the laminate consists of the part above the delamination of thickness  $h$  referred to as the delaminated part and the part below the delamination of thickness  $H = T - h$  referred to as the substrate part. The remaining intact laminate of thickness  $T$  and length  $b = L - \ell$  is referred to as the base plate. Accordingly, the sub-

script  $i = d, s, b$  refers to the delaminated part and the substrate or the base plate, respectively.

The solution in (12) is based on considering the buckled configuration of the delaminated layer as part of an inflectional elastica with end amplitude  $\Phi_d$  and distortion parameter  $\epsilon$ . The distortion parameter represents the tangent rotation at an inflection point from the straight position. At the critical state, the end amplitude is  $\Phi_d^0$ . Suppose that in the slightly buckled configuration,  $\Phi_d$  can be expanded in the form:

$$\Phi_d = \Phi_d^0 + \phi_d^{(1)} \epsilon + \phi_d^{(2)} \epsilon^2 + O(\epsilon^3). \tag{7}$$

Then the end rotation at the common section  $\theta$  is given by expanding the relevant expression (25) in Taylor series in terms of  $\epsilon$  (notice that at the critical state  $\theta^0 = 0$ ):

$$\begin{aligned} \theta &= (\sin \Phi_d) \epsilon - \frac{1}{24} (\sin \Phi_d \cos^2 \Phi_d) \epsilon^3 + \dots \\ &= (\sin \Phi_d^0) \epsilon + (\cos \Phi_d^0) \phi_d^{(1)} \epsilon^2 \\ &\quad + \left[ (\cos \Phi_d^0) \phi_d^{(2)} - (\sin \Phi_d^0) \frac{\phi_d^{(1)2}}{2} \right. \\ &\quad \left. - \frac{1}{24} \sin \Phi_d^0 \cos^2 \Phi_d^0 \right] \epsilon^3 + \dots \\ &= \theta^{(1)} \epsilon + \theta^{(2)} \epsilon^2 + \theta^{(3)} \epsilon^3 + O(\epsilon^4). \end{aligned} \tag{8}$$

Because of the continuity condition,  $\theta$  is the same for both the delaminated and substrate parts as well as the base plate. Asymptotic expansions for the end moment,  $M_d$ , the axial force  $P_d$  and the flexural contraction,  $f_d$ , are similarly found by substituting Eq 7 into the relevant expression (25) and subsequently expanding in Taylor series.

Although the substrate part and the base plate undergo moderate bending with no inflection point, we may also use the elastica theory to describe their (non-linear) deformation; and in this case the inflection points are outside the actual elastic curve. For the substrate part we have to expand not only the amplitude  $\Phi_s$  but also the distortion parameter  $\alpha_s$  in a perturbation series with respect to the distortion parameter of the delaminated layer  $\epsilon$ :

$$\Phi_s = \Phi_s^0 + \phi_s^{(1)} \epsilon + \phi_s^{(2)} \epsilon^2 + O(\epsilon^3), \tag{9a}$$

$$\alpha_s = \alpha_s^{(1)} \epsilon + \alpha_s^{(2)} \epsilon^2 + \alpha_s^{(3)} \epsilon^3 + O(\epsilon^4). \tag{9b}$$

The amplitude at the common section,  $\Phi_b$  and the distortion parameter,  $\alpha_b$ , of the base plate are also expanded in terms of the distortion parameter of the delaminated part,  $\epsilon$ . This allows an expansion of the end moments  $M_s, M_b$ , the axial forces,  $P_s$  and  $P$  and the flexural contractions  $f_s$  and  $f_b$  in terms of  $\epsilon$ .

Having obtained the asymptotic expressions for the force and deformation quantities, the equilibrium and compatibility requirements that ultimately define the nonlinear post-critical path are the force and moment equilibrium at the common section and a condition

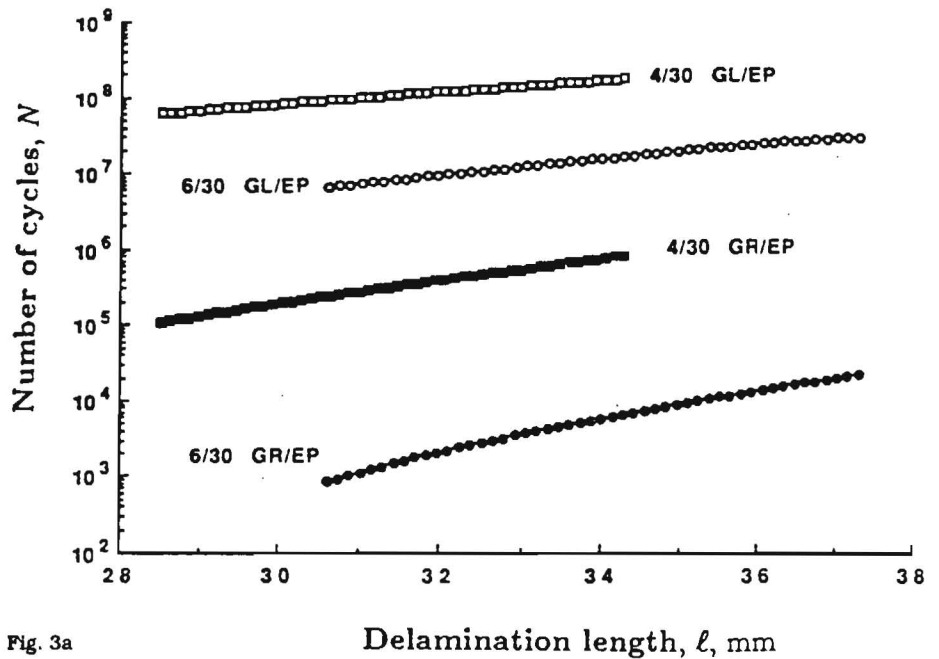


Fig. 3a

Fig. 3a. Comparison of the predicted fatigue delamination growth,  $N - l$  (semilogarithmic plot), for the glass/epoxy and graphite/epoxy cases.  
 Fig. 3b. Comparison of the energy release rate at  $\epsilon_{max}$ ,  $G_{max} = G_{max}/\Gamma_0(\psi)$ , versus delamination half-length,  $l/l_0$ , for the glass/epoxy and graphite/epoxy cases.

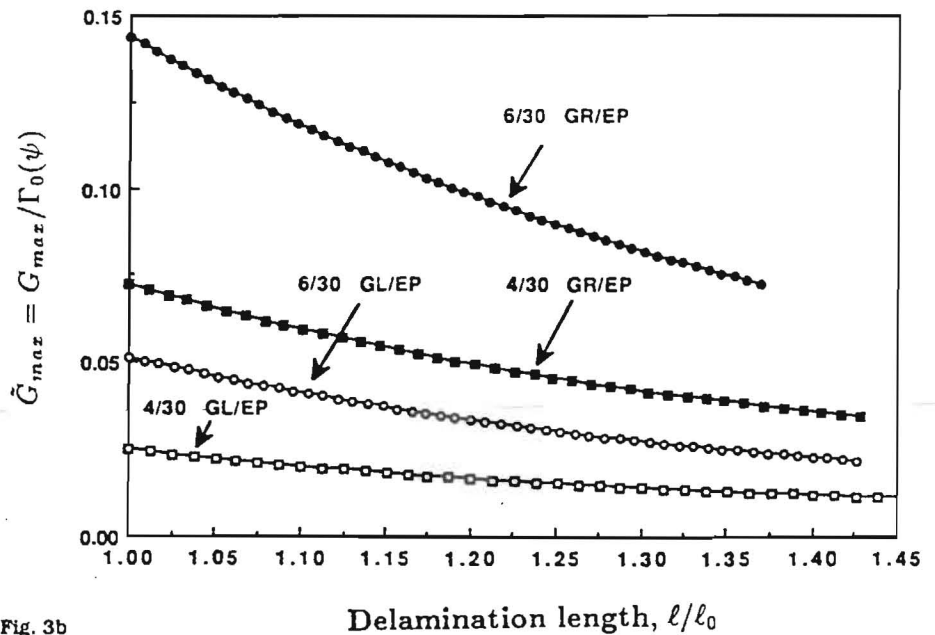


Fig. 3b

that involves the compatible shortening of the delaminated and substrate parts. These conditions are imposed for the first, second, and third order terms separately and lead to: (a) one nonlinear equation for the zero order terms, which defines the critical point (characteristic equation), (b) two linear algebraic equations for  $\phi_d^{(1)}$  and  $\phi_s^{(1)}$  that determine the first order forces, and (c) two linear algebraic equations for  $\phi_d^{(2)}$  and  $\phi_s^{(2)}$  that define the second order forces (12).

The initial postbuckling solution that has just been briefly described is used in conjunction with the interface crack solutions summarized by Hutchinson and Suo (23). For a general bimaterial interface crack, these solutions depend on the Dundurs (26) parameters,  $\bar{\alpha}$ ,  $\bar{\beta}$  and the bimaterial constant  $\bar{\epsilon}$ . For the ho-

mogeneous system under consideration,  $\bar{\alpha} = \bar{\beta} = \bar{\epsilon} = 0$ .

For the plane-strain interface crack shown in Fig. 4, the energy release rate,  $G$ , is:

$$G = \frac{1}{2E_L} \left[ \frac{P^{*2}}{Ah} + \frac{M^{*2}}{Ih^3} + 2 \frac{P^* M^*}{\sqrt{AI}h^2} \sin \gamma \right] \quad (10a)$$

where  $P^*$  and  $M^*$  are linear combinations of the loads from the previous postbuckling solution:

$$P^* = P_d - C_1 P - C_2 \frac{M_b}{h} \quad (10b)$$

$$M^* = M_d - C_3 M_b \quad (10c)$$

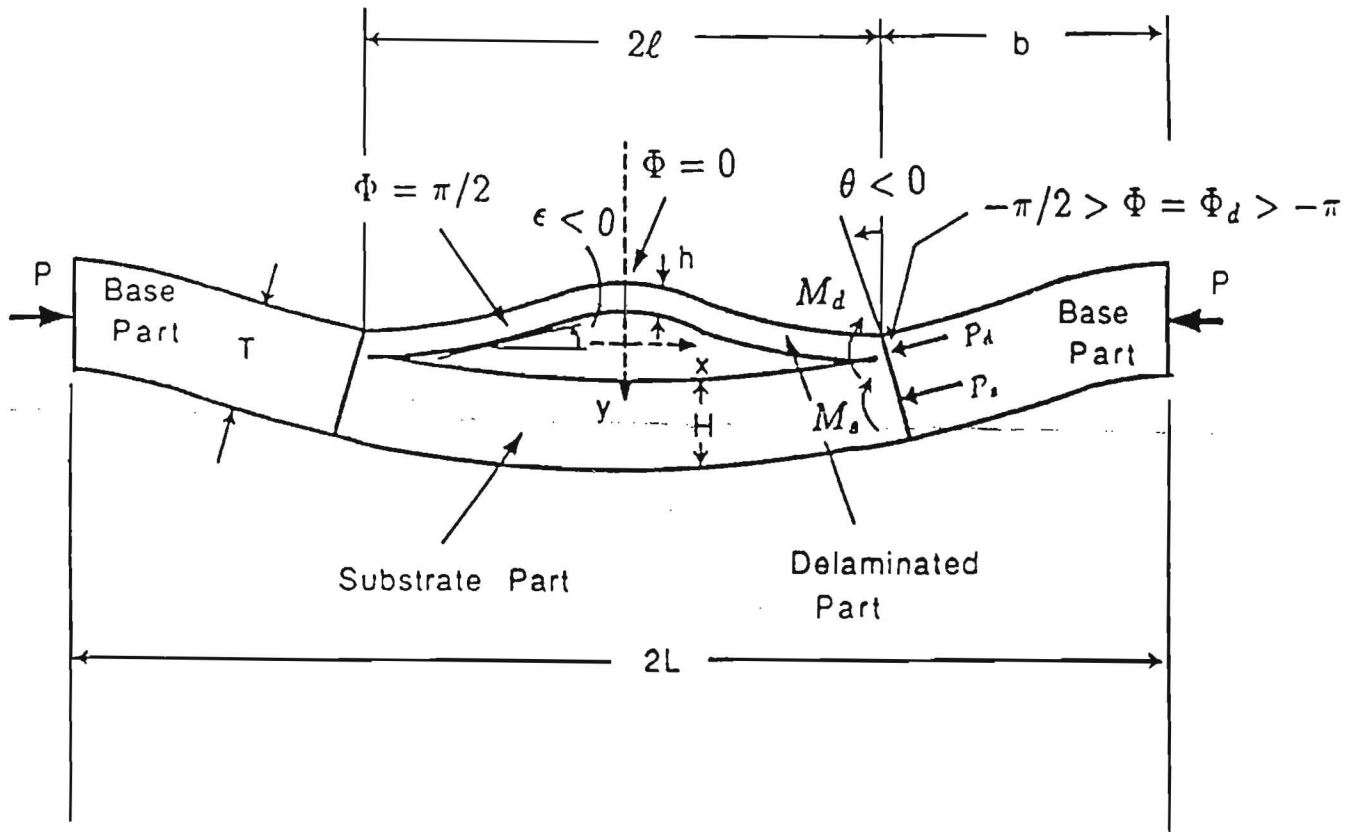


Fig. 4. A compressively loaded one-dimensional delamination configuration in the post-critical state.

The constants  $C_1, C_2, C_3, A, I$  and the angle  $\gamma$ , restricted such that  $\gamma \leq \pi/2$ , are in terms of the dimensions,  $h$  and  $H$  (23). The preceding formula does not separate the opening and shearing components. Instead, the following two expressions give the Mode I and Mode II stress intensity factors:

$$K_I = \frac{1}{\sqrt{2}} \left[ \frac{P^*}{\sqrt{Ah}} \cos \omega + \frac{M^*}{\sqrt{Ih^3}} \sin(\omega + \gamma) \right], \quad (11a)$$

$$K_{II} = \frac{1}{\sqrt{2}} \left[ \frac{P^*}{\sqrt{Ah}} \sin \omega - \frac{M^*}{\sqrt{Ih^3}} \cos(\omega + \gamma) \right]. \quad (11b)$$

Accurate determination of  $\omega$ , which depends only on  $\eta$  (for a fixed set of Dundurs constants  $\bar{\alpha}, \bar{\beta}$ ), requires the numerical solution of an integral equation and has been reported in Suo and Hutchinson (14). The extracted  $\omega$ , however, varies slowly with the ratio  $h/H$  in the entire range  $0 \leq \eta \leq 1$ , in accordance with the approximate formula (23):

$$\omega = 52.1^\circ - 3^\circ(h/H). \quad (11c)$$

These formulas are adequate since we are dealing with macroscopically homogeneous material (unidirectional glass/epoxy). For general nonhomogeneous laminated composites with arbitrary stacking sequence the formulas by Sheinman and Kardomateas (16) could be used.

Substituting the asymptotic expressions for the

forces and moments from the postbuckling solution already presented, gives

$$P^* = \epsilon P^{*(1)} + \epsilon^2 P^{*(2)} + \dots, \quad M^* = \epsilon M^{*(1)} + \epsilon^2 M^{*(2)} + \dots \quad (12a)$$

Now the energy release rate and the Mode I and II stress intensity factors can be written in the form:

$$G = \epsilon^2 G^{(2)} + \epsilon^3 G^{(3)} + \dots, \quad (12b)$$

$$K_{I,II} = \epsilon K_{I,II}^{(1)} + \epsilon^2 K_{I,II}^{(2)} + \dots \quad (12c)$$

The other quantity that is needed to correlate with the experiments is the applied strain,  $\epsilon_0$ , which is the external loading quantity. This is given as follows:

$$\epsilon_0 = \epsilon_0^{(0)} + \epsilon_0^{(1)} \epsilon + \epsilon_0^{(2)} \epsilon^2, \quad (13a)$$

where (12):

$$\epsilon_0^{(0)} = \frac{P^0}{ET}; \quad \epsilon_0^{(1)} L = \frac{P^{(1)}b}{ET} + \frac{P_d^{(1)}\ell}{Eh} + \frac{H}{2} \theta^{(1)}, \quad (13b)$$

$$\epsilon_0^{(2)} L = \frac{f_d^{(2)}}{2} + \frac{P_d^{(2)}\ell}{Eh} + f_b^{(2)} + \frac{P^{(2)}b}{ET} + \frac{H}{2} \theta^{(2)}. \quad (13c)$$

The initial postbuckling solution just outlined defines at each level of delamination length and applied compressive strain the resultant forces and moments at the section where the delamination starts; this in

turn defines the energy release rate and the mode mixity, which are used in conjunction with the fatigue delamination growth law to produce through a numerical integration the predicted delamination extension versus number of applied cycles.

### CONCLUSIONS

Experimental results were presented on the fatigue growth of internal delaminations that undergo delamination buckling under cyclic constant amplitude compression in glass/epoxy composite beam/plates. The growth of the delaminations takes place under mixed mode conditions characterized by a relatively high value of the Mode II component, which is increasing as the delaminations grow. In a similar fashion as in the graphite/epoxy material, the fatigue delamination growth in these glass/epoxy specimens is affected by the relative location of the delamination through the plate thickness, the fatigue growth being slower for a smaller value of delamination thickness over plate thickness (delaminations located closer to the surface). A mode-dependent cyclic growth law is used and is shown to provide adequate correlation with the experiments. A comparison of the cyclic growth rate in glass/epoxy specimens with the corresponding one in graphite/epoxy specimens of the same geometry and applied loading, shows that the delamination would grow much faster in the graphite/epoxy specimens. Furthermore, the graphite/epoxy would be in a state of higher energy release rate values for the same applied  $\epsilon_{max}$ . The mode mixities, however, are nearly the same in both the glass/epoxy and graphite/epoxy cases for the same geometry.

### ACKNOWLEDGMENT

The authors are grateful to Dr. T. Kevin O'Brien of NASA Langley for donating the glass/epoxy material that was used in the experiments. Furthermore, the financial support of the Office of Naval Research, Ship Structures and Systems, S&T Division, Grant N00014-91-J-1892, and of the Army Research Office (ARO) through the Georgia Tech Center of Excellence for Rotary Technology (CERT), Grant DAAL 03-93-G-0002 are both gratefully acknowledged, as well as the interest and encouragement of the Grant monitors, Dr. Yapa Rajapakse and Dr. Gary Anderson.

### REFERENCES

1. G. A. Kardomateas and D. W. Schmueser, *AIAA Journal*, **26**, 337 (1988).
2. H. Chai, C. D. Babcock, and W. G. Knauss, *Int. J. Solids Struct.*, **17**, 1069 (1981).
3. G. J. Simitzes, S. Sallam, and W. L. Yin, *AIAA Journal*, **23**, 1437 (1985).
4. A. G. Evans and J. W. Hutchinson, *Int. J. Solids Struct.*, **20**, 455 (1984).
5. I. Sheinman and M. Adan, *J. of Appl. Mech.*, (ASME), **54**, 558 (1987).
6. K.-F. Nilsson and B. Storåkers, *J. of Appl. Mech.*, (ASME), **59**, 530 (1992).
7. G. A. Kardomateas, *J. Compos. Technol. Res.*, (ASTM), **12**, 85 (1990).
8. A. J. Russell and K. N. Street, in *Toughened Composites*, ASTM STP 937, pp. 275-94, American Society for Testing and Materials, Philadelphia (1987).
9. A. J. Russell and K. N. Street, in *Composite Mater.: Testing and Design*, ASTM STP 972, pp. 259-77, American Society for Testing and Materials, Philadelphia (1988).
10. T. K. O'Brien, in *Composite Mater.: Testing and Design (Ninth Volume)*, ASTM STP 1059, pp. 7-33, S. P. Garbo, ed., American Society for Testing and Materials, Philadelphia (1990).
11. H. Chai, *Exp. Mech.*, 296 (1992).
12. G. A. Kardomateas, *J. Appl. Mech.* (ASME), **60**, 903 (1993).
13. G. A. Kardomateas and A. A. Pelegri, "Growth Behavior of Internal Delaminations in Composite Plates Under Compression: Effect of the End Conditions," *Int. J. Fracture* vol. 75, pp. 49-67, 1996.
14. Z. Suo and J. W. Hutchinson, *Int'l J. Fracture*, **43**, 1 (1990).
15. W.-L. Yin and J. T. S. Wang, *J. Appl. Mech.*, **51**, 939 (1984).
16. I. Sheinman and G. A. Kardomateas, "Energy Release Rate and Stress Intensity Factors for Delaminated Composite Laminates," *Int. J. Sol. Struct.* vol. 34, No. 4, pp. 451-459, 1997.
17. G. A. Kardomateas and A. A. Pelegri, *Int'l J. Fracture*, **65**, 261 (1994).
18. G. A. Kardomateas, A. A. Pelegri and B. Malik, "Growth of Internal Delaminations Under Cyclic Compression in Composite Plates" *J. Mech. Phys. Sol.* vol. 43, No. 6, pp. 847-868, 1995.
19. G. B. Murri and R. H. Martin, in *Compos. Mater.: Fatigue and Fracture, Fourth Volume*, ASTM STP 1156, pp. 239-56, W. W. Stinchcomb and N. E. Ashbaugh, eds., American Society for Testing and Materials, Philadelphia (1993).
20. T. K. O'Brien, G. B. Murri, and S. A. Salpekar, in *Composite Materials: Fatigue and Fracture, Second Volume*, ASTM STP 1012, pp. 222-50, Paul A. Lagace, ed., American Society for Testing and Materials, Philadelphia (1989).
21. Y. J. Prel, P. Davies, M. L. Benzeggagh, and F-X de Charentenay, in *Composite Materials: Fatigue and Fracture, Second Volume*, ASTM STP 1012, pp. 251-69, Paul A. Lagace, ed., American Society for Testing and Materials, Philadelphia (1989).
22. K. M. Liechti and Y. S. Chai, *J. Appl. Mech.*, (ASME), **59**, 295 (1992).
23. J. W. Hutchinson and Z. Suo, in *Advances in Applied Mechanics*, **29**, 63, Academic Press, New York (1992).
24. C. Bathias and A. Laksimi, in *Delamination and Debonding of Materials*, ASTM STP 876, pp. 217-37, W. S. Johnson, ed., American Society for Testing and Materials, Philadelphia (1985).
25. S. J. Britvek, *The Stability of Elastic Systems*, Pergamon, New York (1973).
26. J. Dundurs, *Mathematical Theory of Dislocations*, pp. 70-115, American Society of Mechanical Engineering, New York (1969).